Chemical Engineering Journal 159 (2010) 149–158

Contents lists available at ScienceDirect

Chemical Engineering Journal

journal homepage: www.elsevier.com/locate/cej

# Numerical and experimental study on flue gas desulfurization in the underfeed circulating spouted bed

Min Tao, Baosheng Jin*, Wenqi Zhong*, Yaping Yang, Rui Xiao

*School of Energy and Environment, Southeast University, Nanjing 210096, China*

ARTICLE INFO

*Article history:*
Received 6 November 2009
Received in revised form 13 January 2010
Accepted 31 January 2010

*Keywords:*
Underfeed circulating spouted bed
Flue gas desulfurization
Multi-level humidifying
Numerical simulation

ABSTRACT

An underfeed circulating spouted bed (UCSB) reactor was used as a desulfurization apparatus. In this study, an attempt was made to build a mathematical 3D model which couples the complicated flow and chemical reactions in the interest of system analysis and sulfur removal data analysis. A simplified reaction model was developed to describe the $SO_2$ absorption process. Humidifying, evaporation, neutralization reaction have been considered in the model while the dissolution and ionization of calcium hydroxide are neglected. The effect of operating parameters including feed style, injecting velocity, jet water flow rate, humidifying style on sulfur removal efficiency were investigated. The results show that the calculation gives a good description of the experimental data under the range of operating conditions. It indicates that the model is successful in predicting the desulfurization efficiency of the UCSB system.



## 1. Introduction

The underfeed circulating spouted bed (UCSB), which feeds the sorbent particles by spouting, is designed as a dry desulfurization reactor. The main objective of the technology is to improve particle distribution and strength solid mixing in the riser. Compared with conventional fluidized bed which feeds the sorbent particles from the side of the riser, the gas–solid contact in the UCSB can be more uniform and sufficient. The intense solid mixing not only provides the even choice for gas–solid contact, but also removes the product layer of recycling material. This will be of great benefit to advancing the desulfurization efficiency and calcium utilization.

A large number of studies were performed to develop mathematic model to predict the desulfurization efficiency by dry/semi-dry absorption with calcium hydroxide agent [1–3]. Neathery [4] proposed a semi-empirical model based on the assumptions of isothermal and the plug flow in the reaction bed. Tan et al. [5] applied a mathematic model by means of infinitesimal method to simulate the evaporation process during the desulfurization. Yan et al. [6] proposed a model to simulate the process characteristic of circulating fluidized bed-flue gas desulfurization (CFB-FGD) and conducted a detailed analysis to investigate the influences of operating parameters on the sulfur removal efficiency. However, most of the models neglect the complex flow behavior in the riser. Wang et al. [7] deduced a particle-flow-passage model to simulate the impaction humidification process between particles and droplets in the desulfurization process. A comprehensive 3D model was established with the models of gas phase turbulence, heat and mass transfer, and the chemical reactions being considered. However, this method of microcosmic modeling is overloaded with details and might be inefficient for engineering prediction. Therefore, the aim of our work is to develop a simplified model that can simulate the flow behavior as well as the desulfurization reaction in the reactor more efficiently. In this study, the prediction is compared to the experimental results to validate the improvement on desulfurization efficiency by the underfeed style. The model will be useful for prediction and analysis of the desulfurization performance and as a tool for design and optimization of the flue gas desulfurization processes.

## 2. Experimental system

The experiments were conducted in an underfeed circulating spouted bed-flue gas desulfurization (FGD) system, which consists of seven major sections: (1) flue gas generation system; (2) reaction bed; (3) humidifying system; (4) underfeed system; (5) recycling system; (6) separation system; (7) measurement system. The experimental setup of the UCSB-FGD system is shown schematically in Fig. 1. The reaction bed consists of an insulated steel pipe 0.6 m in diameter and 15 m in length. A total of 6 sampling ports are positioned at the reactor wall throughout the height of the riser. The inlet and outlet concentrations of $SO_2$ were measured by a flue gas analyzer (SAE19, MRU). And the gas temperature was investigated through thermocouples.

Flow through the system is maintained by two blowers, one located upstream of the reaction bed and the other downstream

* Corresponding authors. Tel.: +86 25 83794744; fax: +86 25 83795508.
*E-mail addresses:* bsjin@seu.edu.cn (B. Jin), wqzhong@seu.edu.cn (W. Zhong).

1385-8947/$ – see front matter © 2010 Elsevier B.V. All rights reserved.
doi:10.1016/j.cej.2010.01.057

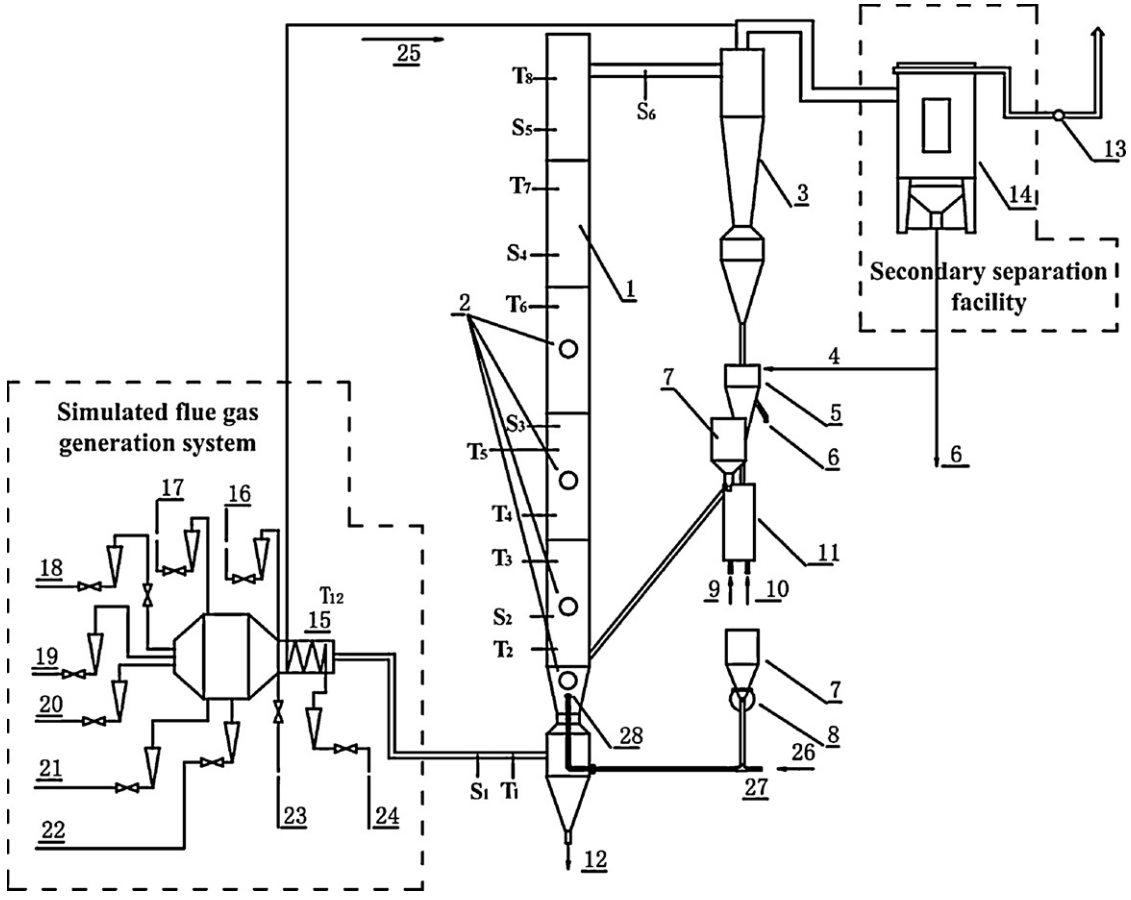


**Fig. 1.** Schematic diagram of the underfeed circulating spouted bed-flue gas desulfurization system.

of the bag filter. This 'push–pull' arrangement is used to minimize excessive pressure or vacuum within the riser. The flue gas generation system provides heated simulated flue gas through the combustion of diesel oil in the burner. Sulfur dioxide may be injected to the simulated gas at any desired concentration. The composition of original flue gas is shown in Table 1. For humidifying, domestic water was applied and added by two-fluid sprayers. The sprayers are located at heights of 1.0, 3.0, 5.0 and 7.0 m above the venture tube, respectively and the jet water flow rate is controlled by a calibrated rotameter. The droplet diameter is between 20 and 150 μm.

The sorbent served in the experiment contains 90.39% of calcium hydroxide with an average diameter of 80 μm and density of 2300 kg/m$^3$. Applying the facefeed style, the calcium hydroxide agent is added by the screw feeder connecting with the loop seal. For the underfeed style, the underfeed system is applied. The fresh agent in the barrel hopper is first translated into the injector. Then the particles are pushed by high speed gas and finally injected into the bottom bed from the underfeed nozzle. The underfeed nozzle used in the experiment contains four orifices of Ø10 mm. The head of the nozzles is a taper of 120° so as to avoid particle accumulation.

**Table 1**
Composition of original flue gas.

| Chemical composition | Unit | Concentration |
|---|---|---|
| $O_2$ | % | 20.1 |
| CO | ppm | 5 |
| $CO_2$ | % | 0.6 |
| $NO_x$ | ppm | 3 |
| $H_2S$ | ppm | – |

The distance from the center of nozzle to the bottom of divergent cone can be adjusted at 0.3 or 0.5 m for the pipeline is connected by the pipe unions which can be moved easily. At default conditions, the nozzle was located at the height of 0.3 m from the bottom of divergent cone.

## 3. Mathematical model

### 3.1. Basic principles

In the UCSB system, the sorbent powder and the work water were injected into the reactor, respectively. During the humidifying, the sorbent powder collided with the water droplets and was then covered by a liquid film. Concentrated slurry droplets were formed as a result of the inertial impactions between sorbent powder and water droplets [7]. So the desulfurization and evaporation processes are very similar to the spray-dry method. The sulfur dioxide absorption process can be schematized as a series of steps [8]:

(i) Gas phase diffusion of $SO_2$ from the gas bulk to the droplets surface.
(ii) Dissolution of $SO_2$ at the droplet surface.
(iii) Formation of sulfurous acid and dissociation into ionic sulfur species following the scheme:

$$SO_{2(aq)} + H_2O \Rightarrow H_2SO_{3(aq)}$$
$$H_2SO_{3(aq)} \Leftrightarrow H^+ + HSO^-_{3(aq)}$$
$$HSO^-_{3(aq)} \Leftrightarrow H^+ + SO^{2-}_{3(aq)}$$

(iv) Diffusion of sulfur species towards the droplet center.
(v) Dissolution and diffusion of calcium hydroxide particles in the droplet.
(vi) Neutralization reaction between acid and alkaline species.

For prediction, it is difficult and time-consuming to simulate such complicated process involving evaporation, ionization, dissolution, neutralization and deposition in the turbulent solid–gas flow. In order to simplify the calculation, the physical and chemical process in the riser is generalized by four steps instead.

(i) Evaporation of the droplet, the reaction rate is referred in literature [9]. The diameter of the droplets is set empirically according to the droplet size atomized in the reactor:

$$H_2O_{(l)} \Rightarrow H_2O_{(g)}$$

(ii) The droplets associates with the calcium hydroxide. Such combination is able to react with sulfur dioxide and this step represents the process of dissolution and ionization. The reaction is considered to be instant and the stoichiometric coefficient of reactant, $n$, is determined by the solubility of the calcium hydroxide:

$$nH_2O_{(l)} + Ca(OH)_2 \Rightarrow Ca(OH)_2 \cdot nH_2O$$

(iii) Absorption of $SO_2$ by the combination. The calculation of reaction rate is referred in literature [10]:

$$Ca(OH)_2 \cdot nH_2O + SO_2 \Rightarrow CaSO_3 + (n+1)H_2O_{(l)}$$

(iv) The water in the droplets continue vaporizing in the riser, so this step is necessary. The evaporation rate is equal to the first reaction:

$$Ca(OH)_2 \cdot nH_2O \Rightarrow Ca(OH)_2 + nH_2O_{(g)}$$

The following assumptions are considered and have been involved in the model:

(1) The moisture keeps vaporizing within the riser.
(2) The reaction between solid calcium hydroxide and sulfur species is very little and can be neglected.
(3) The reaction is activated only in wet condition. In the model, only combination of calcium hydroxide and liquid water contributes to the sulfur absorption.

Since the encounter of various reactants is necessary to the absorption, the humidifying style and distribution uniformity of reactants appear to be very important to the reaction efficiency. Therefore the model gives stress to the resultant effect of mass and heat transfer and passes over detailed physical and chemical steps such as dissolution and ionization. The absorption rate is generalized and controlled by the third reaction instead.

### 3.2. Basic fluid flow and heat transfer

The equation for conservation of mass, or continuity equation, can be written as follows [11]:

$$\frac{\partial \rho}{\partial t} + \nabla(\rho v) = S_m \tag{1}$$

The source $S_m$ is the mass added to the continuous phase.

Conservation of momentum is described by

$$\frac{\partial(\rho v)}{\partial t} + \nabla(\rho v v) = -\nabla p + \nabla(\tau) + \rho g + F \tag{2}$$

with [11]

$$\tau = \mu[\nabla v + (\nabla v)^T] - \frac{2}{3}(\nabla \cdot v)I \tag{3}$$

where $p$ is the static pressure, $\tau$ is the stress tensor, $\rho g$ and $F$ are the gravitational body force and external body forces, respectively, $\mu$ is the molecular viscosity, $I$ is the unit tensor, and the second term on the right-hand side is the effect of volume dilation.

The energy equation is solved in the following form [12]:

$$\frac{\partial(\rho E)}{\partial t} + \nabla(v(\rho E + p)) = \nabla[k_{eff}\nabla T - \sum_i h_i J_i + (\tau_{eff} v)] + S_h \tag{4}$$

where $k_{eff}$ is the effective conductivity, and $J_i$ is the diffusion flux of species $i$. The first three terms on the right-hand side represent energy transfer due to conduction, species diffusion, and viscous dissipation, respectively. $S_h$ includes the heat of chemical reaction and other volumetric heat sources.

The standard $k$–$\varepsilon$ turbulence model is applied in the calculation. It is a semi-empirical model based on model transport equations for the turbulence kinetic energy ($k$) and its dissipation rate ($\varepsilon$). The $k$ and $\varepsilon$ are obtained from the following transport equations:

$$\frac{\partial}{\partial t}(\rho k) + \nabla \cdot (\rho v k) = \nabla \cdot \left( \left( \mu + \frac{\mu_t}{\sigma_k} \right) \nabla k \right) + G_k + G_b - \rho\varepsilon \tag{5}$$

$$\frac{\partial}{\partial t}(\rho \varepsilon) + \nabla \cdot (\rho v \varepsilon) = \nabla \cdot \left( \left( \mu + \frac{\mu_t}{\sigma_\varepsilon} \right) \nabla \varepsilon \right) + \frac{\varepsilon}{k}(C_{1\varepsilon}G_k - C_{2\varepsilon}\rho\varepsilon) \tag{6}$$

where $G_k$ represents the generation of turbulence kinetic energy due to the mean velocity gradients. $G_b$ is the generation of turbulence kinetic energy due to buoyancy.

The turbulent viscosity, $\mu_t$, is computed by combining $k$ and $\varepsilon$ as follows:

$$\mu_t = \rho C_\mu \frac{k^2}{\varepsilon} \tag{7}$$

The model constants $C_{1\varepsilon}$, $C_{2\varepsilon}$, $C_\mu$, $\sigma_k$ and $\sigma_\varepsilon$ were found to be 1.44, 1.92, 0.09, 1.0 and 1.3, respectively. These default values have been determined from experiments with air and water for fundamental turbulent shear flows including homogeneous shear flows and decaying isotropic grid turbulence. They have been found to work fairly well for a wide range of wall-bounded and free shear flows.

### 3.3. Species transport equations

The local mass fraction of each species, $Y_i$, is predicted through the solution of a convection–diffusion equation for the $i$th species. This conservation equation takes the following general form [13]:

$$\frac{\partial}{\partial t}(\rho Y_i) + \nabla \cdot (\rho v Y_i) = -\nabla J_i + R_i + S_i \tag{8}$$

where $R_i$ is the net rate of production by chemical reaction and $S_i$ is the rate of creation by addition from the dispersed phase.

In turbulent flows, the mass diffusion is computed in the following form:

$$J_i = -\left( \rho D_{i,m} + \frac{\mu_t}{Sc_t} \right) \nabla Y_i \tag{9}$$

where $Sc_t$ is the turbulent Schmidt number, $\mu_t/\rho D_t$, with a default setting of 0.7.

### 3.4. The generalized finite-rate formulation for reaction modeling

Except the steps of evaporation and neutralization, the reaction rates that appear as source terms are computed by the finite-rate model. In the finite-rate model, the effect of turbulent fluctuations is ignored, and reaction rates are determined by Arrhenius expressions. The net source of chemical species $i$ due to reaction $R_i$ is computed as the sum of the Arrhenius reaction sources over the $N_R$ reactions that the species participate in:

$$R_i = M_{w,i}\sum_{i=1}^{N_R}\hat{R}_{i,r} \tag{10}$$

where $M_{w,i}$ is the molecular weight of species $i$ and $\hat{R}_{i,r}$ is the Arrhenius molar rate of creation of species $i$ in reaction $r$. Consider the $r$th reaction written in general form as follows:

$$\sum_{i=1}^{N} v'_{i,r}M_i \xrightarrow{k_{f,r}} \sum_{i=1}^{N} v''_{i,r}M_i$$

where $N$ is the number of chemical species in the system, $v'_{i,r}$ is the stoichiometric coefficient for reactant $i$ in reaction $r$, $v''_{i,r}$ is the stoichiometric coefficient for product $i$ in reaction $r$, $M_i$ is the symbol denoting species $i$ and $k_{f,i}$ is the forward rate constant for reaction $r$.

The molar rate of creation/destruction of species $i$ in reaction $r$ is given by [14–16]

$$\hat{R}_{i,r} = (v''_{i,r} - v'_{i,r})\left(k_{f,r}\prod_{j=1}^{N_r}[C_{j,r}]^{\eta'_{j,r}}\right) \tag{11}$$

where $N_r$ is the number of chemical species in reaction $r$, $C_{j,r}$ is the molar concentration of each reactant and product species $j$ in reaction $r$, $\eta'_{j,r}$ is the forward rate exponent for each reactant and product species $j$ in reaction $r$.

The forward rate constant for reaction $r$, $k_{f,r}$, is computed using the Arrhenius expression [17,18]

$$k_{f,r} = A_r T^{\beta_r} e^{-E_r/RT} \tag{12}$$

where $A_r$ is the pre-exponential factor, $\beta_r$ is the temperature exponent, $E_r$ is the activation energy for the reaction and $R$ is the universal gas constant.

### 3.5. Simulation considerations

The simulation grid is shown in Fig. 2. In the calculation domain, the number of grids was 107,702. Among these grids, the minimum area was $1.310\times10^{-4}\,m^2$, and the maximum area was $3.487\times10^{-3}\,m^2$. The model was mainly divided with quad shape grid. The grids were thickened locally at areas near the atomizers and the underfeed nozzle as shown in the figure.

The model was calculated through commercial CFD code Fluent 6.2. The CFD software provides a user-defined function (UDF), with which the software can be used in various applications. In this work, UDF was used to program the chemical reaction rate equations. For the boundary conditions, we selected the velocity-inlet condition for the inlet of the reactor and the outflow condition for the outlet of the reactor. At the walls, a zero gradient condition was used for the turbulent kinetic energy. The no-slip wall condition was used for the gas phase [19]. The calculation of species transport and chemical reaction was based on the solution of transport equations for species mass fractions, with the chemical reaction mechanism defined. The reaction rates that appeared as source terms in the species transport equations were computed from

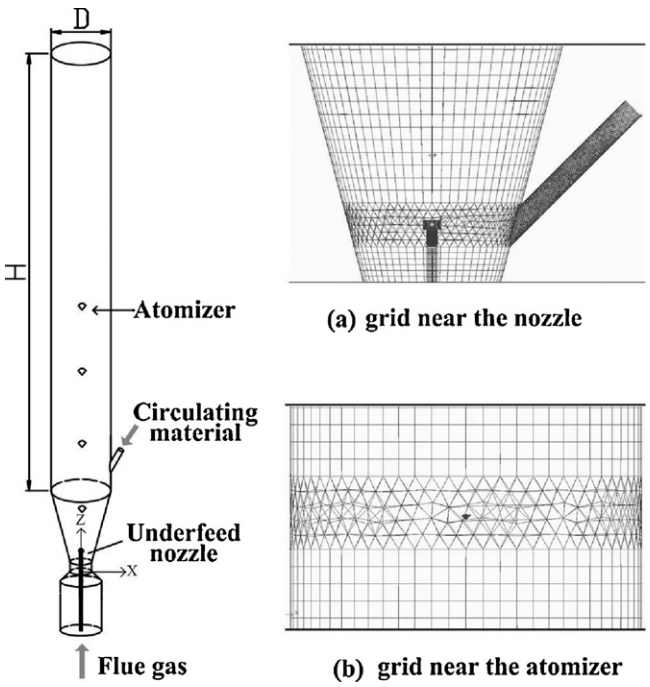


**Fig. 2.** Picture of the model and simulation grid.

Arrhenius rate expressions. All of the simulations were corresponding to experimental operations. For the evaluation of the convective terms, the second order QUICK (quadratic upwind interpolation of convective kinematics) scheme was used. During the calculation, computational time of about 120 min is required for each operation condition.

## 4. Results and discussion

### 4.1. The influence of feed style on desulfurization efficiency

Fig. 3 shows the simulated results of concentration distribution of calcium hydroxide in the riser with different feed styles. The operation parameters of corresponding experiments are listed as follows: the flue gas flux was 1831 N m$^3$/h. The inlet flue gas was 140 °C with $SO_2$ concentration of 773.4 ppm and the Ca/S molar ratio was 1.3. The total jet water flow rates were 52 kg/h and 2-level humidifying was applied in both feed styles. According to the calculations, the feed style has obvious influence on species distribution. As the fresh desulfurization agent is added from the side face with the facefeed style, the concentration distribution of calcium hydroxide is dissymmetrical on the section. The agent concentrates on the right side especially in the bottom of the riser as shown in Fig. 4a. This leads to disadvantage to sulfur removal for the humidifying area in the bottom bed is the main zone where desulfurization reaction takes place.

Applying the underfeed style, the fresh agent was added from the underfeed nozzle which located in the center of the riser, therefore, the species distribution gets more symmetrical as shown in Fig. 4b. Meanwhile, the high speed injecting flow near the underfeed nozzle has a cutting and reforming effect on the flow field. As a result, the species mixing is strengthened and the removal effect of $SO_2$ gets better as shown in Fig. 5. It is seen in Fig. 6 that the concentration distribution of $SO_2$ with underfeed style is also glossier than the facefeed style.

The simulated results of desulfurization efficiency are shown in Fig. 7. It is seen from the figure that the removal efficiency (RE) of $SO_2$ with underfeed style is evidently higher than that with face-

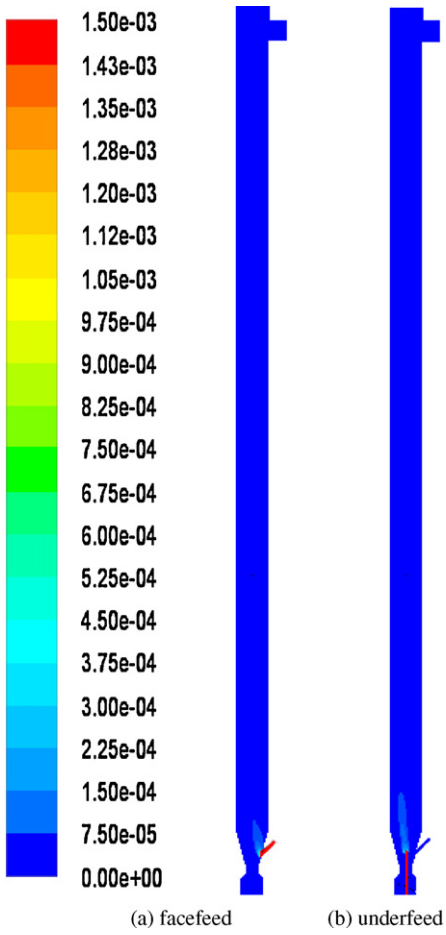


**Fig. 3.** Concentration distribution of $Ca(OH)_2$ on the section (kmol/m$^3$). (a) Facefeed and (b) underfeed.

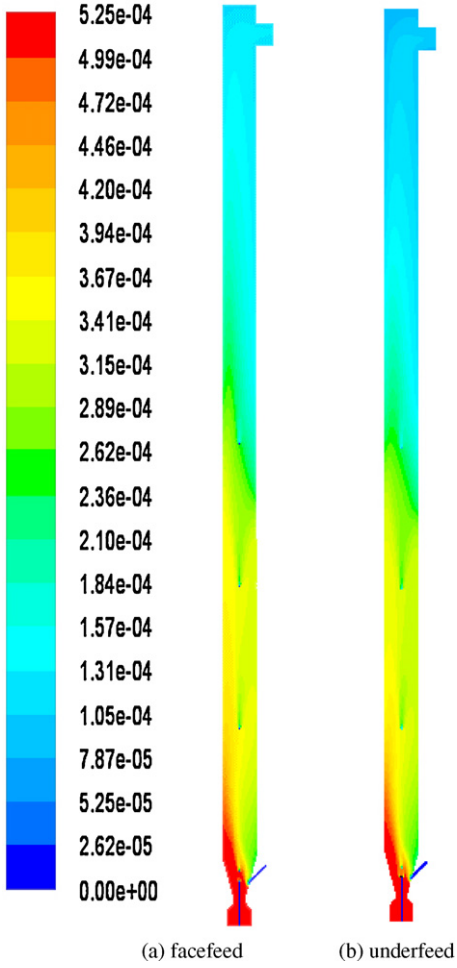


**Fig. 5.** Molar fraction of $SO_2$ on the vertical section. (a) Facefeed and (b) underfeed.

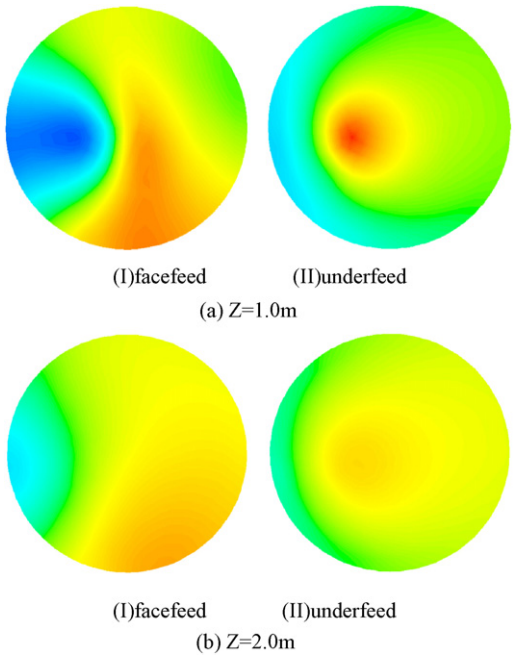


**Fig. 4.** Concentration distribution of $Ca(OH)_2$ on the cross-section (kmol/m$^3$). (a) $Z$ = 1.0 m and (b) $Z$ = 2.0 m.

feed style. The calculations also validated the conclusion. It should be noted that the desulfurization effect of recycling material was not considered in the model, therefore, the simulation results are evidently lower than the experimental data.

### *4.2. The influence of injecting velocity on desulfurization efficiency*

The results of simulations reveal the effect of injecting velocity (gas velocity at outlet of the underfeed nozzle) on flow field and species distribution as shown in Figs. 8 and 9. The flue gas flux was 1831 N m$^3$/h. The inlet flue gas was 140 °C with $SO_2$ concentration of 773.4 ppm and the Ca/S molar ratio was 1.3. Two-level humidifying was applied with total jet water flow rate of 52 kg/h. From the calculations, the flow field changes and the species distribution improves with higher injecting velocity in the bottom of the riser. Such effect will be even distinct in the magnification of reactors. However, the diameter of the studied riser was quite small comparing with the engineering application. As a result, the influence of injecting velocities on desulfurization efficiency is not very evident. As shown in Fig. 10, when the injecting velocity increases from 15.0 to 20.0 m/s, the RE increases from 79.7% to 80.0% according to the experimental data. Two possible reasons are responsible for this change. One reason is that the mass transfer is more adequate due to the intense turbulence caused by the injecting flow. It can be seen from Fig. 8 that the turbulent intensity increases as the injecting velocity advances. The other reason is related to the fact that species distribution in the riser gets better with higher turbulence.

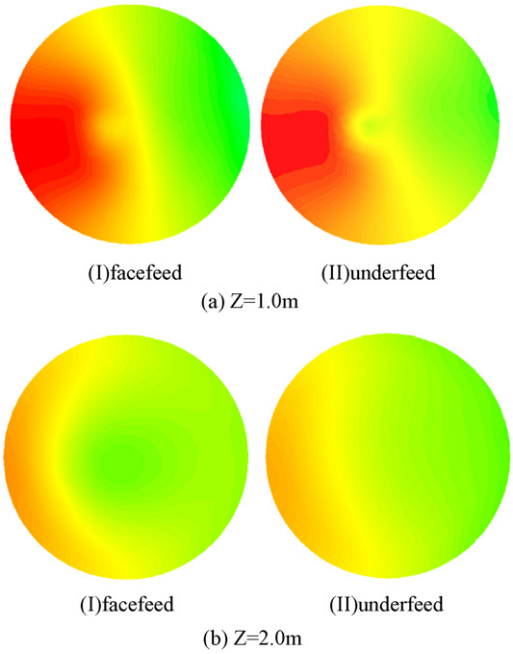


**Fig. 6.** Molar fraction of $SO_2$ on the cross-section. (a) $Z$ = 1.0 m and (b) $Z$ = 2.0 m.

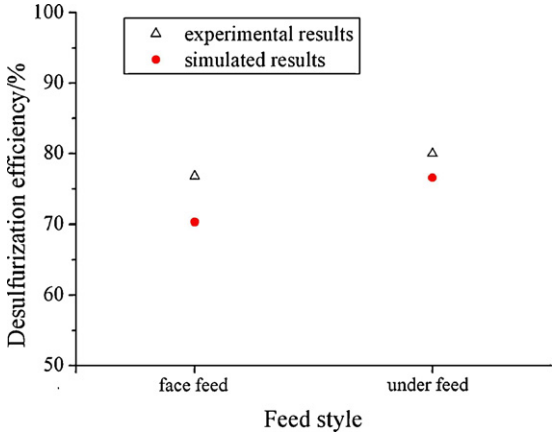


**Fig. 7.** Experimental and simulated results of desulfurization efficiency with different feed styles.

The contrast of concentration distribution of calcium hydroxide at different injecting velocities is evident as shown in Fig. 9. Therefore, it can be concluded that the high injecting velocity is beneficial to desulfurization reaction.

In the practical operation, the intense solid mixing in the UCSB can remove the product layer of recycling material and thus to improve the calcium utilization. However, this process was not considered in the model. As a result, the influence of injecting velocity on the desulfurization efficiency is undervalued in the calculation.

### 4.3. The influence of work water flow rate on desulfurization efficiency

The work water flow rate is one of the most important operating parameters affecting the performance of the desulfurization. Flue gas humidifying has distinct effects on advancing the activation of calcium hydroxide. As the moisture in the droplets exceeds the critical value, the desulfurization mechanism changes. The desulfurization process turns to ionic reactions between $OH^-$, $Ca^{2+}$, $HSO_3^-$,

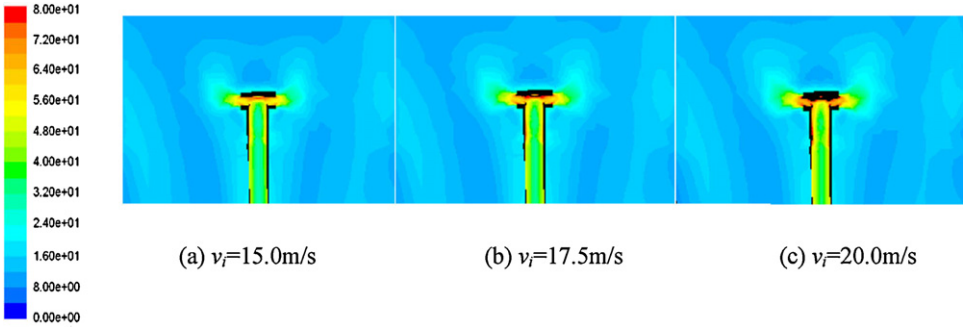


**Fig. 8.** Turbulent intensity near the underfeed nozzle. (a) $v_i$ = 15.0 m/s, (b) $v_i$ = 17.5 m/s, and (c) $v_i$ = 20.0 m/s.

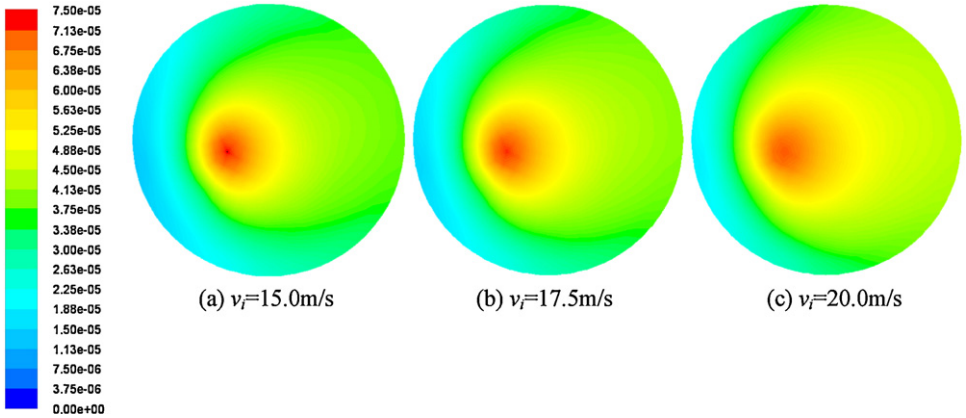


**Fig. 9.** Concentration distribution of $Ca(OH)_2$ at the height of 2.0 m (kmol/m$^3$). (a) $v_i$ = 15.0 m/s, (b) $v_i$ = 17.5 m/s, and (c) $v_i$ = 20.0 m/s.

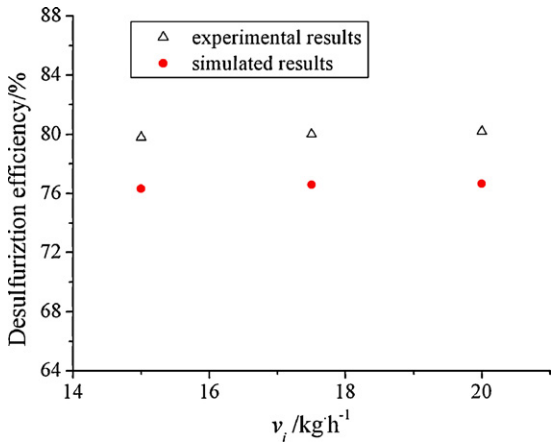


**Fig. 10.** Experimental and simulated results of desulfurization efficiency with different injecting velocities.

$SO_3^{2-}$ and so on in the liquid phase. The desulfurization reaction becomes more efficient because of the reduced diffusion distance and diffusion resistance in the droplet.

The calculation results of concentration distribution of liquid water are shown in Fig. 11. The main operation parameters were the same as above. It is seen that the moisture in the riser ascends obviously as the jet water flow rate advances and as a result, the average temperature gets lower in the riser as shown in Fig. 12. As the temperature descends, the evaporation time of droplets gets longer and the virtual reaction time between ions is prolonged. Meanwhile, the solubility of $SO_2$ in the droplet increases. This is of great benefits to the sulfur removal efficiency. Simulated results of $SO_2$ concentration with different jet water flow rates are as shown in Figs. 13 and 14. It is seen in Fig. 15 that the RE of $SO_2$ increases from 74.1% to 84.8% as the jet water flow rate increases from 42 to 62 kg/h according to the experimental results. The calculation results accords with the experiments very well.

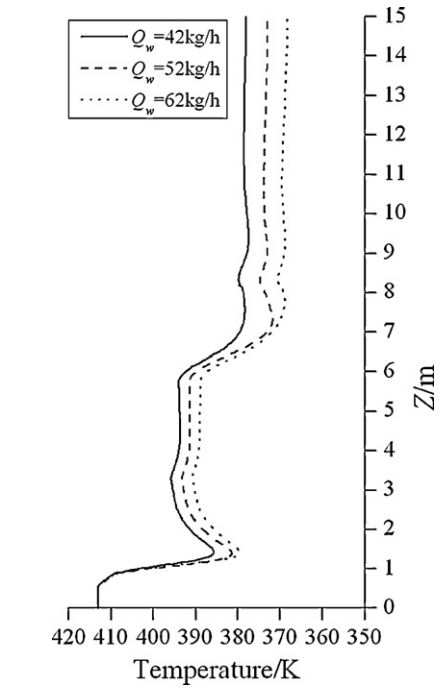


**Fig. 12.** Change of gas phase temperature along the axial direction.

### 4.4. The influence of humidifying style on desulfurization efficiency

Fig. 16 shows the simulated results of concentration distribution of liquid water in the riser with different humidifying styles. The main operation parameters were the same as above. The total jet water flow rate was 52 kg/h and the flow rate of each layer was the same while multi-level humidifying was applied. The calcu-

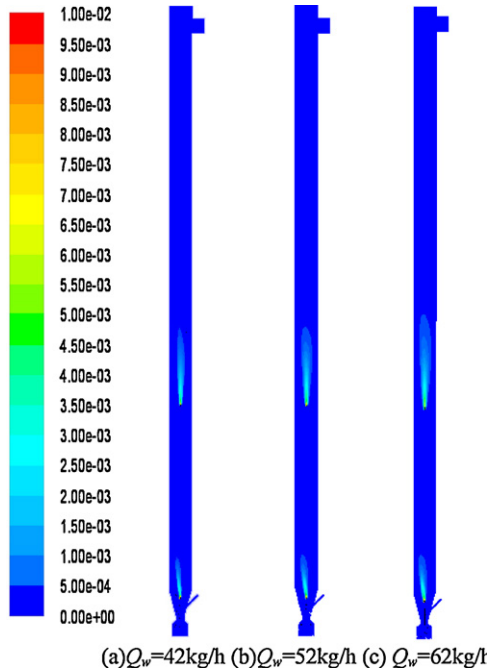


**Fig. 11.** Concentration distribution of liquid water on the vertical section (kmol/m$^3$). (a) $Q_w$ = 42 kg/h, (b) $Q_w$ = 52 kg/h, and (c) $Q_w$ = 62 kg/h.

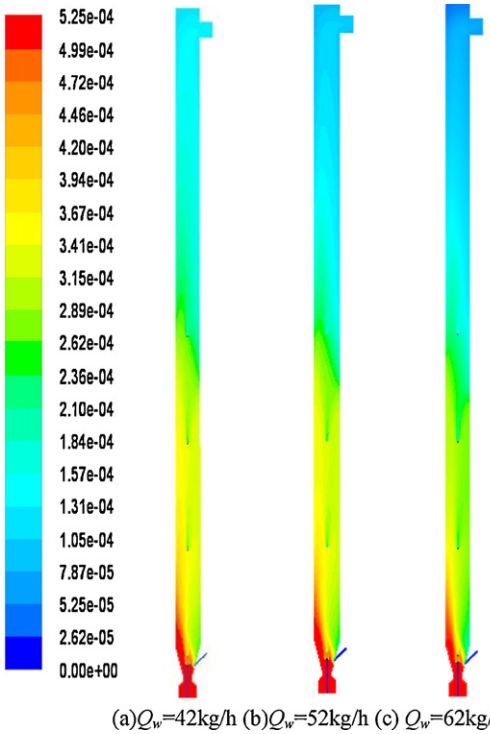


**Fig. 13.** Simulated results of $SO_2$ molar fraction with different jet water flow rates. (a) $Q_w$ = 42 kg/h, (b) $Q_w$ = 52 kg/h, and (c) $Q_w$ = 62 kg/h.

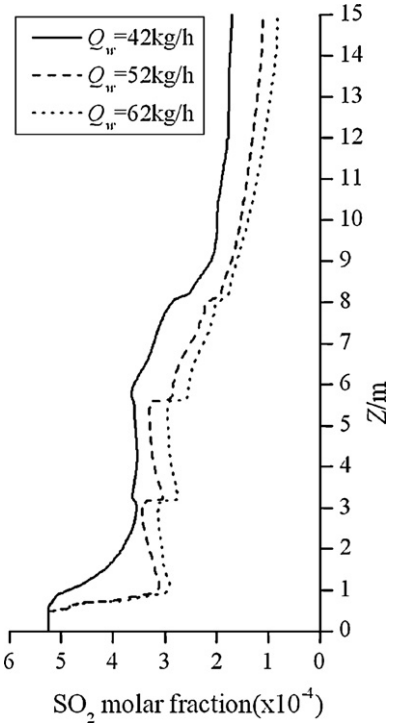


**Fig. 14.** Change of $SO_2$ molar fraction along the axial direction.

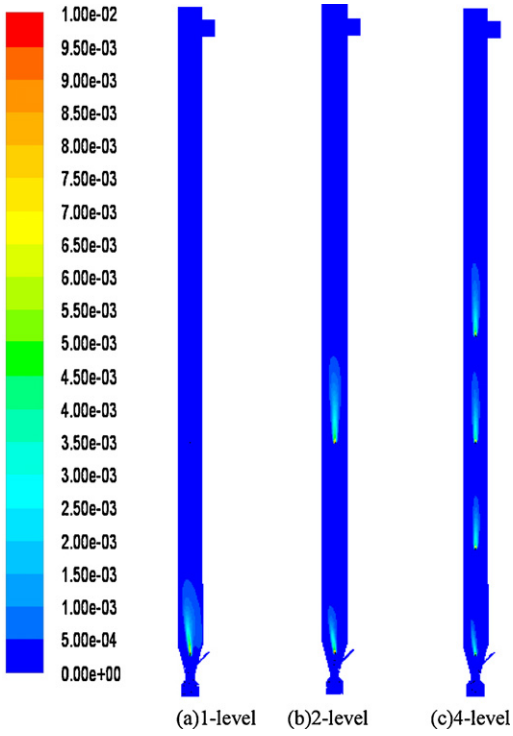


**Fig. 16.** Concentration distribution of jet water on the vertical section (kmol/m$^3$). (a) 1-Level, (b) 2-level, and (c) 4-level.

lation indicates that when applying the multi-level humidifying, the evaporation time of liquid droplets gets longer in the riser. It is seen from Fig. 17 that the outlet temperature of gas phase is lower with multi-level humidifying and the change of temperature is much more tempered. Figs. 18 and 19 shows that the trends of $SO_2$ concentration along the axial direction are similar with the gas temperature. The $SO_2$ concentration drops obviously where the change of temperature is great. It indicates that flue gas humidifying has distinct effects on advancing the activation of calcium hydroxide.

As the temperature field was improved by the multi-level humidifying, the evaporation slowed down and as a result, the desulfurization efficiency increased. It is seen in Fig. 20 that the RE is 72.8% with 1-level humidifying, while RE of 80.0% and 83.6% can be reached applying multi-level style according to the experimental results. The calculations also obtained the same results.

As seen in Table 2, the simulation results are in well agreement with the experimental data (95% confidence interval from 2.90 to 5.65) and the relative errors are within the range of 9.45%. This agreement confirms the usefulness of the supposed model as an effective tool for design and optimization. However, it should be noted that calculation of reaction rate in the model are partially empirical and therefore do not extrapolate data well.

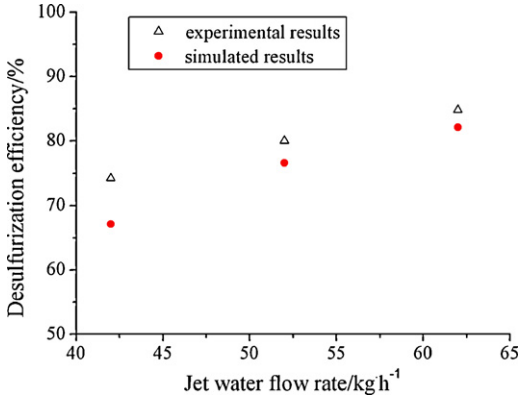


**Fig. 15.** Experimental and simulated results of desulfurization efficiency with different jet water flow rates.

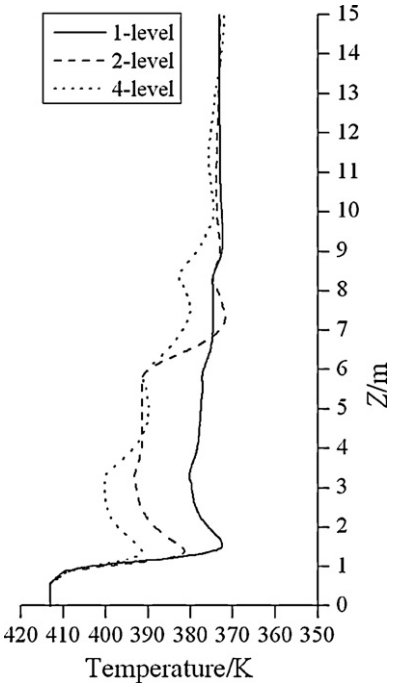


**Fig. 17.** Change of gas phase temperature along the axial direction.

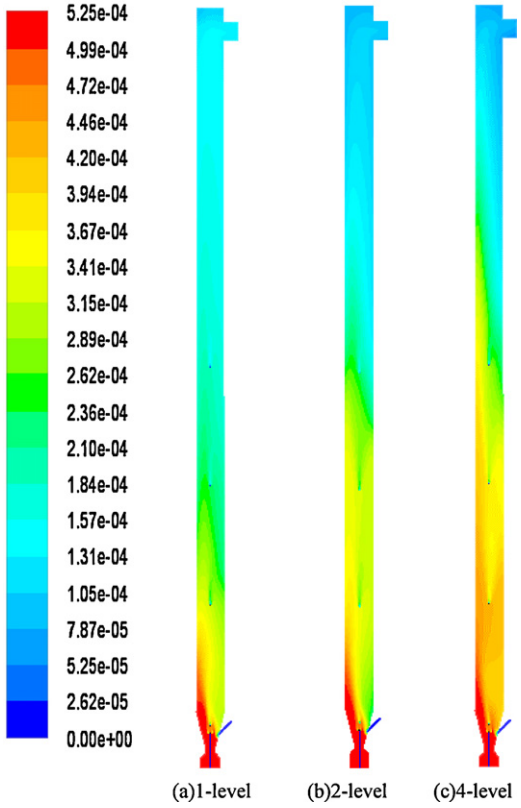


**Fig. 18.** Simulated results of $SO_2$ molar fraction with different humidifying styles. (a) 1-Level, (b) 2-level, and (c) 4-level.

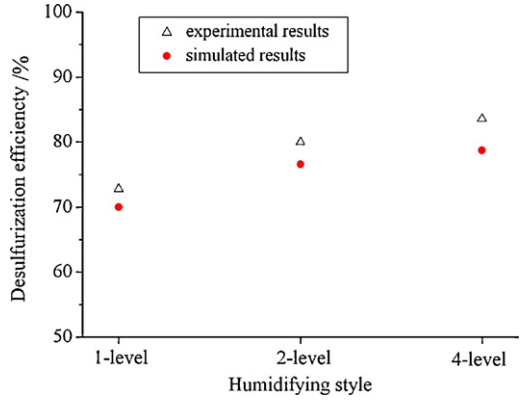


**Fig. 20.** Experimental and simulated results of desulfurization efficiency with different humidifying styles.

**Table 2**
Comparison of experimental and simulated results.

| Sulfur removal efficiency (%) | | Relative error (%) |
|---|---|---|
| Experimental | Predicted | |
| 72.8 | 70.02 | 3.82 |
| 74.1 | 67.10 | 9.45 |
| 76.8 | 70.32 | 8.44 |
| 79.7 | 76.32 | 4.24 |
| 80.0 | 76.58 | 4.28 |
| 80.2 | 76.65 | 4.43 |
| 83.6 | 78.71 | 5.85 |
| 84.8 | 82.13 | 3.15 |

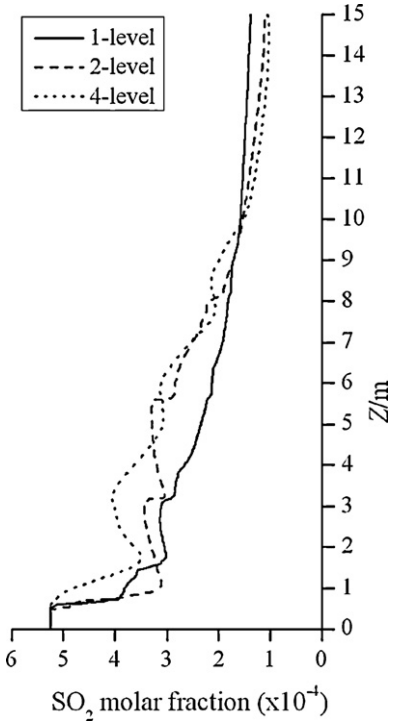


**Fig. 19.** Change of $SO_2$ molar fraction along the axial direction.

## 5. Conclusions

Dry/semi-dry absorption with calcium hydroxide agent is one of the key technologies among current flue gas desulfurization technologies. Numerical simulation is an effective method for scale-up and optimizing the design and operation. In this article, three-dimensional CFD modeling of dry-injection desulfurization with calcium hydroxide in the underfeed circulating spouted bed has been developed, incorporating with the model of species transport, gas phase turbulence, and mass and heat transfer. The distributions of temperature and species composition were presented. The effects of feed and humidifying style on the desulfurization performance were also predicted.

The model shows that the high speed injecting flow near the underfeed nozzle can optimize the flow field and strengthen the mass transfer. The species distribution gets more symmetrical and the sulfur removal efficiency increases when the underfeed style is applied. Advancing the injecting velocity brings on better advantage for sulfur removal. The jet water flow rate and humidifying style are very important operating parameters affecting the performance of the desulfurization. As the jet water flow rate advances, the moisture in the droplets increases and the virtual reaction time between ions is prolonged. Therefore, adequate jet water is crucial factor for high desulfurization efficiency. Appling the multi-level humidifying, the change of temperature in the riser is much more tempered and the RE of $SO_2$ increases.

Comparison of the calculation with the experimental data shows that most of the calculation errors are within the range of 9.45%. This good agreement indicates that the CFD model is useful for prediction and analysis of the desulfurization performance and a powerful tool for design and optimization of the dry/semi-dry desulfurization processes.

## Acknowledgements

Financial supports from the National Key Program of Basic Research in China (No. 2010CB732206) and the National High Technology Research and Development Program of China (No. 2009AA05Z312) were sincerely acknowledged.

## References

[1] M.X. Jiang, T.C. Keener, S.J. Khang, The use of a circulating fluidizing bed absorber for the control of sulfur dioxide emissions by calcium oxide sorbent via in situ hydration, Powder Technology 85 (1995) 115–126.
[2] C.Y. Chu, S.J. Hwang, Attrition and sulfation of calcium sorbent and solids circulation rate in an internally circulating fluidized bed, Powder Technology 127 (2002) 185–195.
[3] F.F. Hill, J. Zank, Flue gas desulphurization by spray dry absorption, Chemical Engineering Process 39 (2000) 45–52.
[4] J.K. Neathery, Model for flue-gas desulfurization in a circulating dry scrubber, AICHE Journal 42 (1996) 259–268.
[5] Z.C. Tan, G.M. Xiang, C.H. Chen, et al., Slurry evaporation of flue gas desulphurization system in circulating fluidized bed, Journal of Tsinghua University 40 (2000) 62–65.
[6] Y. Yan, X.F. Peng, B.X. Wang, Investigation on the transport process of flue gas desulfurization in a circulating fluidized bed, International Communication in Heat Mass Transfer 30 (2003) 71–82.
[7] L. Wang, Y.B. Song, M.C. Zhang, et al., Modeling study on the impaction and humidification process in desulfurization activation reactor, Chemical Engineering Science 60 (2005) 951–962.
[8] F. Scala, M. D'Ascenzo, A. Lancia, Modeling flue gas desulfurization by slurry-dry absorption, Separation and Purification Technology 34 (2004) 143–153.
[9] W.W. Meng, R.W.D. Wan, S.M. Arun, et al., Comparative study of droplet drying models for CFD modeling, Chemical Engineering Research and Design 86 (2008) 1038–1048.
[10] K.T. Lee, O.W. Koon, Modified shrinking unreacted-core model for the reaction between sulfur dioxide and coal fly ash/CaO/$CaSO_4$ sorbent, Chemical Engineering Journal 1 (2008) 1–10.
[11] C.G. Luben, E.M. Fernando, Numerical study on the influence of various physical parameters over the gas–solid two-phase flow in the 2D riser of a circulating fluidized bed, Powder Technology 132 (2003) 216–225.
[12] D.M. Mao, J.R. Edwards, A.V. Kuznetsov, et al., Three-dimensional numerical simulation of a circulating fluidized bed reactor for multi-pollutant control, Chemical Engineering Science 59 (2004) 4279–4289.
[13] Z.Y. Deng, R. Xiao, B.S. Jin, et al., Computational fluid dynamics modeling of coal gasification in a pressurized spouted-fluid bed, Energy & Fuels 22 (2008) 1560–1569.
[14] C.F. Liu, S.M. Shih, R.B. Lin, Kinetics of the reaction of $Ca(OH)_2$/fly ash sorbent with $SO_2$ at low temperatures, Chemical Engineering Science 59 (2004) 1001–1008.
[15] A. Garea, J.L. Herrera, J.A. Marques, et al., Kinetics of dry flue gas desulfurization at low temperatures using $Ca(OH)_2$: competitive reactions of sulfation and carbonation, Chemical Engineering Science 56 (2001) 1387–1393.
[16] I. Fernandez, A. Garea, A. Irabien, Flue-gas desulfurization at medium temperatures—kinetic model validation from thermo-gravimetric data, Fuel 77 (1998) 740–755.
[17] M.J. Renedo, J. Fernandez, Kinetic modeling of the hydrothermal reaction of fly ash, $Ca(OH)_2$ and $CaSO_4$ in the preparation of desulfurant sorbents, Fuel 83 (2004) 525–532.
[18] F.J. Gutierrez Ortiz, P. Ollero, Modeling of the in-duct sorbent injection process for flue gas desulfurization, Separation and Purification Technology 62 (2008) 571–581.
[19] J. Ding, D. Gidaspow, A bubbling fluidization model using kinetic theory of granular flow, AIChE Journal 32 (1990) 523–538.